

Article

Two-Dimensional Zeolitic Imidazolate Framework ZIF-L: A Promising Catalyst for Polymerization

M. Abdur Rahaman ^{1,2,3} , Bibimaryam Mousavi ¹, Farah Naz ^{1,4} and Francis Verpoort ^{1,5,*} 

¹ State Key Laboratory of Advanced Technology for Materials Synthesis and Processing, Wuhan University of Technology, Wuhan 430070, China; md.arch27@gmail.com (M.A.R.); chem_moosavi@yahoo.com (B.M.); farahnaz507@yahoo.com (F.N.)

² School of Materials Science and Engineering, Wuhan University of Technology, Wuhan 430070, China

³ Department of Chemistry, Mawlana Bhashani Science and Technology University, Santosh, Tangail 1902, Bangladesh

⁴ Institute for Advanced Study, Shenzhen University, Shenzhen 518060, China

⁵ National Research Tomsk Polytechnic University, Lenin Avenue 30, 634050 Tomsk, Russia

* Correspondence: francis@whut.edu.cn; Tel.: +86-150-7117-2245

Abstract: Here, for the first time, a 2D and leaf-like zeolitic imidazolate framework (ZIF-L) is reported for the synthesis of ultrahigh molecular weight (UHMW) poly(methyl methacrylate) (PMMA) with M_n up to 1390 kg mol⁻¹. This synthesis method is a one-step process without any co-catalyst in a solvent-free medium. SEM, PXRD, FT-IR, TGA, and nitrogen sorption measurements confirmed the 2D and leaf-like structure of ZIF-L. The results of PXRD, SEM, TGA demonstrate that the catalyst ZIF-L is remarkably stable even after a long-time polymerization reaction. Zwitterionic Lewis pair polymerization (LPP) has been proposed for the catalytic performance of ZIF-L on methyl methacrylate (MMA) polymerization. This MMA polymerization is consistent with a living system, where ZIF-L could reinitiate the polymerization and propagates the process by gradually growing the polymer chains.

Keywords: ultrahigh molecular weight polymer; poly methyl methacrylate; heterogeneous catalyst; zeolitic imidazolate framework



Citation: Rahaman, M.A.; Mousavi, B.; Naz, F.; Verpoort, F.

Two-Dimensional Zeolitic Imidazolate Framework ZIF-L: A Promising Catalyst for Polymerization. *Catalysts* **2022**, *12*, 521. <https://doi.org/10.3390/catal12050521>

Academic Editor: Rubén Mas Ballesté

Received: 19 April 2022

Accepted: 4 May 2022

Published: 6 May 2022

Publisher's Note: MDPI stays neutral with regard to jurisdictional claims in published maps and institutional affiliations.



Copyright: © 2022 by the authors. Licensee MDPI, Basel, Switzerland. This article is an open access article distributed under the terms and conditions of the Creative Commons Attribution (CC BY) license (<https://creativecommons.org/licenses/by/4.0/>).

1. Introduction

Metal-organic frameworks (MOFs), also known as crystalline porous materials, are important discoveries of the 1990s. MOFs have attracted considerable attention over the last two decades due to their special features such as versatile structure, exceptional surface area, and chemical and thermal stability [1–3]. Metal ions or clusters and the enormous variety of organic linkers formulate MOFs structure (2D, 3D) through coordinative bonds and have been exploited in diverse fields, including gas storage and separation, catalysis, sensors, and biomedicine [4–9]. The properties and practical aspects of MOFs mainly depend on their structure, composition and morphology, so it is essential to control the size and morphology of MOF crystals to take full advantage of MOF in diverse applications [10–13].

Tetrahedral metallic ions (Zn and Co) and imidazolate-based organic ligands form a particular class of MOFs, known as zeolitic imidazole frameworks (ZIFs), showing the most desirable characteristics of conventional MOFs and zeolite structures [14]. Some unique properties, including high porosity and surface area, tunable pore size, chemical and thermal stability, make ZIFs an ideal candidate for gas storage, separations, catalysts, biomedical, and energy applications [10,15–20]. In 2013, Wang and his team synthesized a new type of 2D ZIF (known as ZIF-L) with a unique cushion-shaped cavity and leaf-like structure from zinc nitrate hexahydrate and 2-methyl imidazole (2-mIm) in deionized water at room temperature. Subsequently, ZIF-L has attracted significant attention in various applications due to its porous structure and 2D morphology [10,20–24]. This ZIF-L displays

structural similarities in some compositions with 3D ZIF-8, but has different topology, such as in the asymmetric unit. The ZIF-L structure contains two types of Zn^{2+} ions, four 2-mIm linkers and one free 2-mIm molecule where one Zn ion coordinates with four μ_2 -bridging N atoms of two 2-mIm units and another one coordinates with three N atoms of three 2-mIm units and a monodentate one [10,25]. Additionally, in contrast to ZIF-8, the two neighboring 2D SOD layers of ZIF-L are bridged by hydrogen bonding, not by deprotonated 2-mIm, making the ZIF-L's metallic site more readily available than in ZIF-8 [10,26]. Thus, these structural features clarify the effect on the acidic and basic characters of ZIF-L and also inspire us to use them as pairs.

Recently, Lewis pairs components have emerged as new catalysts for various vinyl monomers polymerization, termed Lewis pair polymerization (LPP) [27–29]. In LPP, the Lewis acid (LA) and Lewis base (LB) work simultaneously to activate the monomers and proceeds through activated monomer propagation mechanism via zwitterionic active species to form higher molecular weight polymers [30–32]. However, choosing a suitable combination of LA and LB is still challenging. Furthermore, compared with homogeneous ones, heterogeneous catalysts have the advantage of higher stability, recoverable and reusable properties, and negligible metal contamination in polymer products [33,34]. Meanwhile, several recent studies have demonstrated that ZIF-8 could influence an auspicious catalyst for polymerization due to the presence of LA and LB sites [35–37]; however, despite the presence of Lewis acid and Lewis base sites, there are still no reports of polymerization using ZIF-L. Considering the above results and the scarcity of literature on the topic, we decided to apply the ZIF-L as a polymerization catalyst. Due to the structural system, 2D ZIF (ZIF-L), like other practical applications, seems to be able to perform better than the 3D one (ZIF-8) [21,38–40].

This study reports the bulk polymerization of methyl methacrylate (MMA) by 2D ZIF-L based on zinc metal as a promising catalyst without any solvent and co-catalyst. Indeed, considering the various critical practical aspects of poly (methyl methacrylate) (PMMA), we have chosen MMA for polymerization. Additionally, the polymerization rate of MMA is relatively high among the vinyl monomers. PMMA has emerged as a promising material, especially in lithium polymer batteries as an electrolyte and other potential applications such as biomedical, actuation, optical, and sensor technology [41–47]. Importantly, all of these applications of PMMA depends on its molecular weight. For example, high molecular weight polymer (HMWP)-based gel polymer electrolytes (GPEs) exhibit superior ionic conductivity, good mechanical strength and filming processability. In this case, high molecular weight PMMA has been widely studied as the polymer matrix of GPEs [44,45,48]. Additionally, the biocompatible nature of PMMA enhances its application as bone cement and dental cavity fillings [42]. Although ultrahigh molecular weight (UHMW) PMMA synthesis is still challenging, a few studies have reported the use of high-pressure ($M_n \cong 1250\text{--}3600 \text{ kg mol}^{-1}$) [49,50], high reaction time ($M_n \cong 1927 \text{ kg mol}^{-1}$) [51], aprotic solvent DMSO and tertiary amine N,N,N',N'',N'' -pentamethyldiethylenetriamine (PMDETA) ($M_n \cong 1370 \text{ kg mol}^{-1}$) [52]. Thus, our main goal is to synthesize ultra-high molecular weight poly (methyl methacrylate), using a leaf-like catalyst ZIF-L formed by the green synthesis method, without any co-catalyst, in a solvent free medium.

2. Results and Discussion

2.1. Structural Features of ZIF-L

The synthetic procedure of 2D ZIF-L (Zn) was executed by associating the given amount of $Zn(NO_3)_2 \cdot 6H_2O$ and 2-mIm (1/8 molar ratio of $Zn^{2+}/2\text{-mIm}$) in an aqueous medium at room temperature. Usually, structural purity is one of the characteristics showing the highest catalytic activity of any material. Here, the structural morphology of ZIF-L was examined using several techniques, including SEM, PXRD, FT-IR, TGA, and nitrogen sorption measurements. The results found were in excellent agreement with reported studies [10,53–57]. Figure 1a displays the SEM image of ZIF-L, showing a leaf-like shape with a size of about 4~6 μm length, 1.5~2.5 μm width and of about

200 nm thicknesses [53,54]. The PXRD patterns confirmed the phase purity of ZIF-L with high crystallinity, and the characteristic peaks were consistent with the simulated ones (Figure S1) [22,54,55]. Additionally, compared with the PXRD of ZIF-8, it can be seen that ZIF-L has a similar crystalline structure and an alike pore size inside the 2D crystalline layers [10]. The FT-IR spectrum was recorded to justify the integrity of the ZIF-L structure (Figure 1b). This spectrum can be divided into four parts (from strong to weak peaks), namely, out-of-plane and in-plane bending of the ring, entire ring stretching and N-H...N hydrogen bonds. Among them, the strong to weak peaks at 424, 650–780, 900–1350, 1350–1500, 1566, 2250–3700 cm^{-1} are assigned to Zn-N, out-of-plane bending of the imidazolate ring, in-plane bending of imidazole ring, entire ring stretching, C=N, and N-H...N hydrogen bonds features, respectively [26,55,56]. Two peaks positioned at about 2923 and 3134 cm^{-1} were assigned for the aliphatic and aromatic C-H stretching of the imidazole ring, respectively [58]. Additionally, the aliphatic C-H peaks were observed at 1147 cm^{-1} for the imidazole ring in ZIF-L. Furthermore, in the FT-IR spectrum, a specific peak recorded at 424 cm^{-1} clearly indicates the Zn-N coordination of the formed ZIF-L. The thermal stability of the ZIF-L was scrutinized by using thermogravimetric analysis (TGA) under a nitrogen atmosphere as a function of temperature (Figure S2). The mass residue was observed as about 97.1% at 100 °C, 92.5% at 250 °C and 77.6% at 320 °C, showing signs of removal of a small amount of absorbed water, all guest water molecules and a few weakly bonded ligand molecules, and all weakly bonded ligand molecules, respectively [10,57]. Subsequently, a plateau-sized curve was observed at approximately 320–580 °C, indicating high stability of ZIF-L in the absence of water and 2-mIm. The nitrogen sorption isotherms of ZIF-L exhibit a Type-I shaped isotherm, indicating the presence of a microporous structure (Figure S3). The corresponding results were as follows: BET surface area of 187.25 $\text{m}^2 \text{g}^{-1}$; Langmuir surface area of 203.36 $\text{m}^2 \text{g}^{-1}$; a pore volume of 0.073 $\text{cm}^3 \text{g}^{-1}$ and a pore width of 1.20 nm.

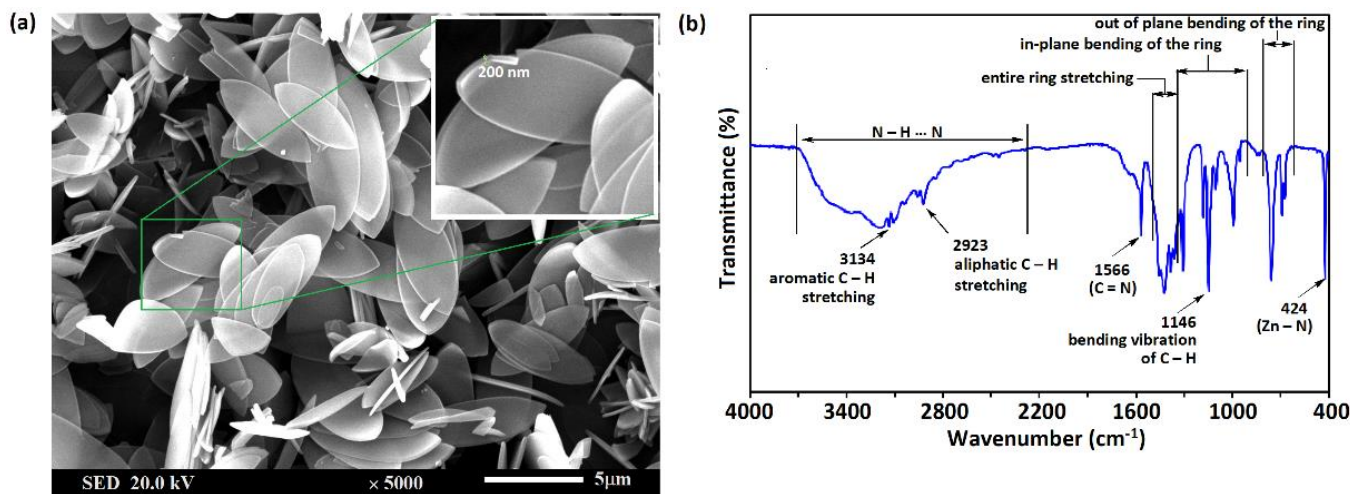


Figure 1. The structural morphology of ZIF-L: (a) SEM image and (b) FTIR spectrum of synthesized ZIF-L.

2.2. Polymerization of MMA

After the ZIF-L was synthesized and characterized, bulk polymerization of MMA was performed at first with ZIF-L to examine the feasibility of ZIF-L as a catalyst at a certain temperature without any co-catalyst in a solvent-free medium. Additionally, numerous zinc salts and 2-mIm (ligand for ZIF-L synthesis) were used under the same conditions. Conversion and molecular weight were checked using ^1H NMR and GPC, respectively (Table S1). These initial studies demonstrated that ZIF-L could act as an effective catalyst for MMA polymerization due to the formation of unprecedented molecular weight of PMMA. Thus, MMA conversion and the ultrahigh molecular weight (UHMW) of PMMA confirm that ZIF-L may be a promising catalyst for MMA polymerization.

In this regard, to explain the catalytic activity levels displayed by ZIF-L, the acidic and basic properties were investigated by temperature program desorption (TPD) technique (Table S2). This method uses NH_3 and CO_2 as gas probe molecules to determine the amount of acidic and basic sites, respectively. Figure 2 displays the NH_3 - and CO_2 -TPD profiles of ZIF-L, where higher acidic sites compared to basic sites indicate the metallic part of ZIF-L is more readily available, which is thought to initiate the polymerization reaction. Various researchers reported that the acidic sites of robust catalyst ZIF-8 are mainly responsible for the polymerization reaction. However, basic sites also contribute to the polymerization process [36,59,60]. Additionally, it can be observed that when the Lewis acid/base ratio is at least 2: 1, then Lewis pairs can effectively polymerize MMA [28,51]. Thus, due to the relatively high acidic character of ZIF-L compared to ZIF-8, it can be assumed that ZIF-L may exhibit higher catalytic performance for MMA polymerization in comparison with ZIF-8 and other reported MOFs.

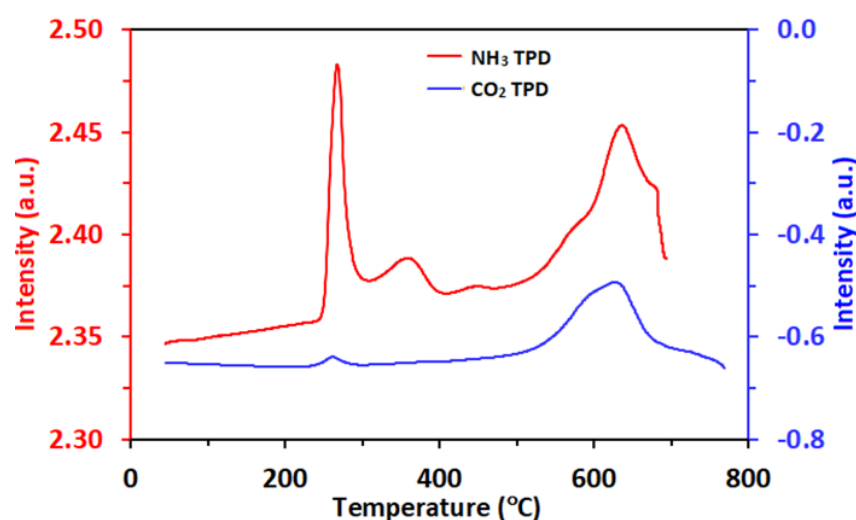


Figure 2. NH_3 -TPD and CO_2 -TPD profiles of the synthesized ZIF-L.

Subsequently, considering the various parameters (such as reaction temperature, polymerization time, monomer/catalyst molar ratio, organic solvents, etc.), the catalytic activity of ZIF-L was investigated elaborately on MMA polymerization, and all of the results are summarized in Table 1. It is noteworthy that the molecular weight of the PMMA increases with increasing temperature and polymerization time but decreases with the molar ratio. Excitingly, a UHMW PMMA was obtained at 24 h and 140 °C temperature. The time-dependent evolution of MMA conversion gives an idea about the constant concentration of the active propagating species in MMA during polymerization (Figure S4). Furthermore, detected results, such as the linear increase in molecular weight with monomer conversion, reveal that MMA polymerization is consistent with a living system, where ZIF-L initiates the polymerization and propagates the process by gradually growing the polymer chains (Figure S5). However, the “livingness” of this synthetic UHMW polymer can be better understood through a chain extension experiment because, in that case, the synthesized UHMW PMMA later reacts with approximately the same amount of monomers (Table S3, Figure S6).

An analysis of the kinetics study revealed that, initially, the polymerization rate increases with the increasing conversion, suggesting first-order kinetics, but deviates from the first-order kinetics as the polymerization rate decreases with time (Figure S7). The existence of progressive viscosity through reaction and its increase over time may be a possible reason. Again, due to the high viscosity, the polymer eventually reaches such a condition where all the constituents lose their segmental mobility. This is why, in very rare cases the polymerization reaction can proceed, but in most of the cases the polymerization stops, resulting in a lot of free monomers in the system [61]. Considering the initial reaction

rate, it would take 19 h for all monomers to be converted to polymers. Still, in reality, it takes much longer than that, as 90% of monomers are converted to polymers in 40 h. As a result, it can be said that due to the formation of HMWP, the viscosity increases and the reaction rate decreases and, hence, slightly deviates from the expected first-order kinetics.

Table 1. Experimental results of MMA polymerization using ZIF-L at various temperatures and MMA/ZIF-L ratio.

Entry	Temp. (°C)	Time (h)	[M]/[Cat]	Conv. ^a (%)	M_n ^b (kg/mol)	\bar{D} ^b
1	100	24	50/1	17	796	1.58
2	120	24	50/1	52	849	1.69
3	140	24	50/1	83	1390	1.12
4	140	3	50/1	20	745	1.78
5	140	6	50/1	38	890	1.37
6	140	12	50/1	64	1080	1.55
7	140	24	100/1	77	1210	1.46
8	140	24	200/1	63	940	1.69
9	140	24	400/1	50	716	1.73
10	140	24	800/1	34	459	1.79
11	140	24	1000/1	27	407	1.57
12 ^c	140	24	50/1	64	632	1.62
13 ^d	140	24	50/1	85	434	1.77

^a conv. = % of MMA conversion calculated by ¹H NMR integration of the methoxy resonance relative intensities of the residual MMA and PMMA in CDCl₃, ^b Determined by gel permeation chromatography (GPC) analysis in THF at RT referenced to polystyrene standards, ^c run with DMF as solvent, ^d run with toluene as solvent.

The analysis of synthesized polymers is very significant for identifying the active sites nature of both monomers and catalysts; therefore, to gain information, conventional techniques were used. Figure 3 shows the ¹H-NMR spectrum of PMMA obtained using ZIF-L. The characteristic peaks of -C(CH₃)(COOCH₃), -CH₂- and -C(CH₃)(COOCH₃) protons were allocated at 0.8–1.4, 1.8–2.1, and 3.62 ppm region, respectively, which are fully consistent with the formation of PMMA. Importantly, the signal at the 1.64 ppm region indicates the presence of a six-membered lactone ring, which may possibly be formed by intramolecular backbiting cyclization during the chain-termination step [62,63]. In this case, comparatively higher acidity of the catalyst may assist the formation of lactone (Figure S8) [29]. Although the UHMW PMMA formation approves the chain growth reaction, there may be chain termination at the end of the polymerization, as evidenced by the presence of a peak in the 1.64 ppm region. Again, the values related to the UHMW PMMA reveal that the rate of polymerization at the initiation and chain-propagation steps is significantly higher compared to the backbiting reaction. Moreover, the presence of -OH group in the polymer structure is proved by the signals at 2.90 and 2.98 ppm, which is additionally affirmed by the acid anhydride method (Figure S9) [64]. The absence of the FT-IR peak at 1639 cm⁻¹, assignable to the C = C double bond in the PMMA, reveals the formation of a C-C single bond in the PMMA (Figure S10). In addition, the vinyl peak at 941 cm⁻¹ in the MMA spectrum drifted to 988 cm⁻¹ for PMMA, suggesting living polymerization characteristics. Additionally, DSC analysis of PMMA (Table 1, entry 3), determined under N₂ flow, exposes that the glass transition temperature (T_g) of the synthesized PMMA is 124.8 °C (Figure S11).

Furthermore, a series of ions were observed from the MALDI-TOF MS spectrum from the low molecular weight PMMA, where intervals of the mass ions were equal to the molar mass of MMA, i.e., equal to the repeating unit of PMMA (Figure 4). Specifically, a plot of m/z values of the series against the number of MMA repeat unit (n) provided a straight line with a slope of 100.07 (corresponds to the molar mass of the monomer, MMA) and an intercept of 435.76, corresponding to a six-membered lactone ring as the chain end. Thus, the above results confirm the synthesized PMMA is a linear polymer with ZIF-L/lactone chain ends. Additionally, ICP analysis discloses that PMMA contains approximately 0.0005% Zn, which is very small and negligible.

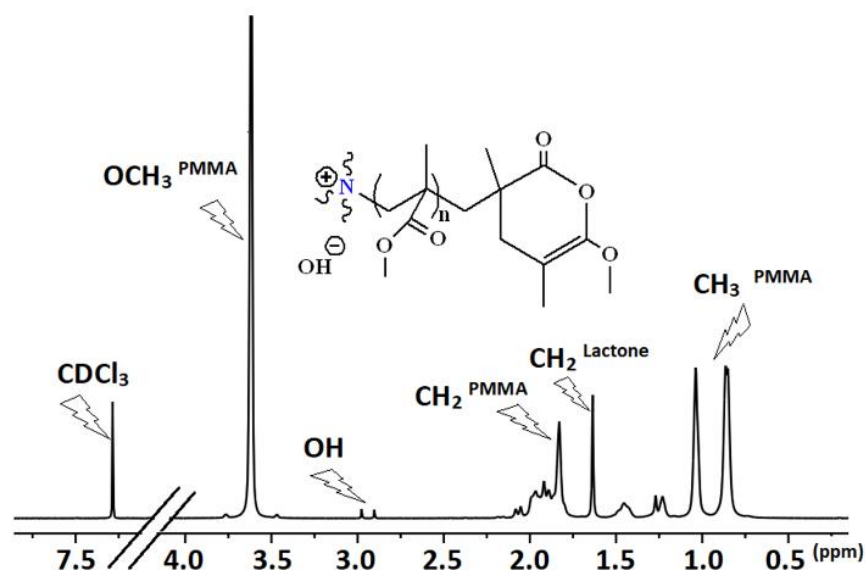


Figure 3. $^1\text{H-NMR}$ spectrum of PMMA in CDCl_3 obtained using ZIF-L at 140°C (Table 1, entry 3).

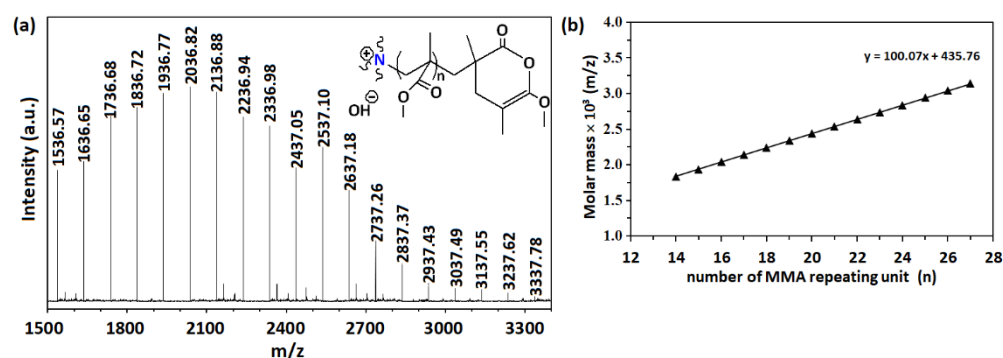
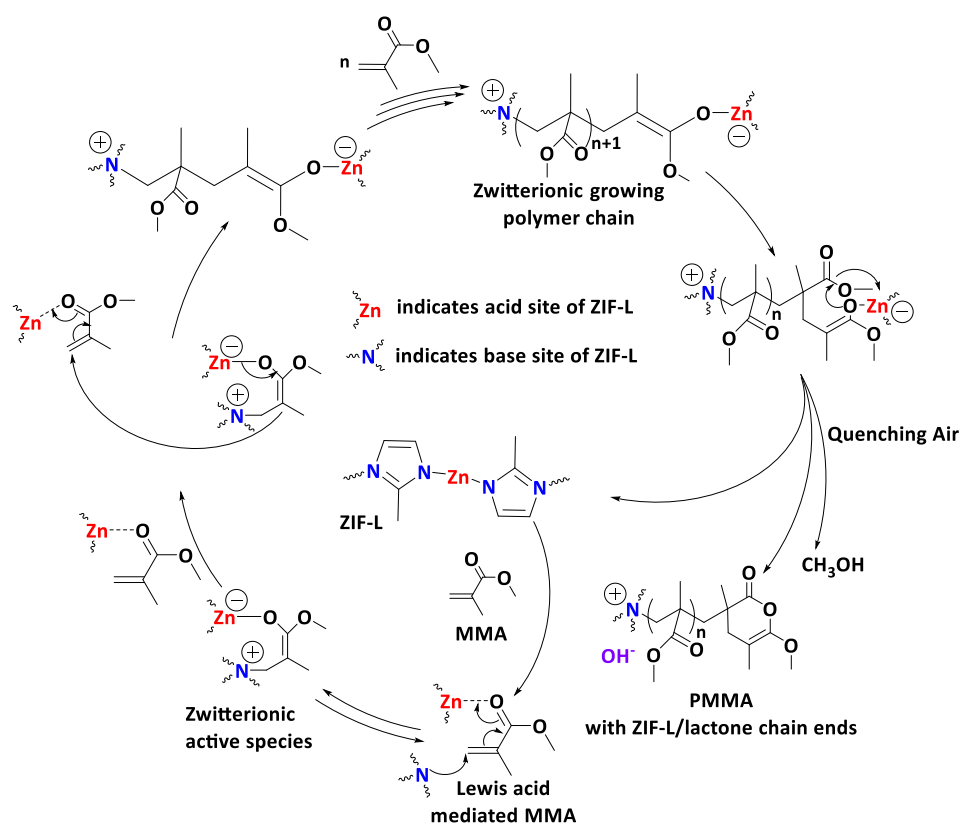


Figure 4. Low-MW PMMA obtained by using ZIF-L at 140°C : (a) MALDI-TOF mass spectrum, (b) plot of m/z values against the number of MMA repeating units (n).

Based on the above experimental details and literature reports, we proposed the zwitterionic Lewis pair polymerization (LPP) mechanism for the catalytic performance of ZIF-L on MMA polymerization (Scheme 1). Following the two activation steps, a zwitterionic active species is formed at the initiation, where first, the Lewis acid (LA) sites of the catalysts bind with free monomers to form activated monomers. Then, the Lewis base (LB) sites attack the activated monomers to form zwitterionic active species. Some earlier studies reported that zwitterionic active species do not react with free monomers in the case of Lewis pairs mediated polymerization [28,32,65]. So, propagation would then proceed by the addition of zwitterionic active species with the LA-activated monomer. The continuous addition of MMA to this activated species would give rise to the chain growth of polymerization. Finally, the experimentally obtained LB bounded PMMA with a six-membered lactone ring chain end would result regarding the backbiting cyclization reaction under air exposure [63]. Importantly, LB-bound polymer chains with lactone ring (six-membered) cannot polymerize newly added monomers, although, under inert medium, it can polymerize new monomers through chain extensions. This observation suggests that chain termination through the formation of a lactone ring (six-membered) chain end occurred only at air exposure.



Scheme 1. Proposed zwitterionic Lewis pair polymerization mechanism for the polymerization of MMA using ZIF-L.

2.3. Recoverability and Reusability of Catalyst

Recoverability and reusability are significant characteristics of heterogeneous catalysts. Therefore, in this study, these properties of ZIF-L were investigated. For this purpose, the polymerization reaction was carried out on a large scale in the Schlenk flask. After a certain period, the catalyst was collected by filtration from the reaction mixture, washed several times, dried under vacuum overnight, and reused to check the efficiency of the catalyst. Importantly, PXRD (Figure S12), SEM (Figure S13), and BET (Figure S14) analysis of the recovered ZIF-L after the third cycle confirms the stability of the ZIF-L during polymerization. Additionally, leaching of Zn ions in the reaction mixture was analyzed after the first and third cycle using the ICP technique and, conspicuously, very slight leaching of Zn ions was observed (Table S4). Since there is a relationship between the stability and catalytic performance of heterogeneous catalysts, recovered ZIF-L was reused for the MMA polymerization to investigate the catalytic activity under identical conditions (Table S5). From the experimental results, it is confirmed that there was no significant change in the catalytic activity of the recovered ZIF-L after at least three cycles for MMA polymerization. The slightly lower molecular weight (M_n) compared to using a fresh catalyst (ZIF-L) indicates minor structural change during long-time polymerization, which can be said to be negligible.

3. Materials and Methods

3.1. Materials

Methyl methacrylate (MMA; 99%), 2-methylimidazole (2-mIm; 99%), and ethyl 2-bromo-2-methylpropanoate (EBiB; 98%) were purchased from Aladdin Chemical Co., Ltd. and $\text{Zn}(\text{NO}_3)_2 \cdot 6\text{H}_2\text{O}$ (>98%) from Macklin. At the beginning, MMA was first dried over CaH_2 and then distilled at a reduced pressure at 50 °C (two times distillation) and, after

that, preserved under an inert atmosphere. All reagents and solvents were used as received from commercial suppliers (Aladdin, TCI) without further purification.

3.2. Synthesis of Catalyst ZIF-L

Following the procedure reported elsewhere, 2D ZIF-L(Zn) crystals were synthesized in an aqueous system at room temperature [10]. In the ZIF-L synthesis system, the ratio $\text{Zn}^{2+}/2\text{-mIm}$ in aqueous solution plays an important role because a higher ratio facilitates the formation of ZIF-8 [66,67]. In a typical procedure, $\text{Zn}(\text{NO}_3)_2 \cdot 6\text{H}_2\text{O}$ (0.595 g, 2 mmol) was dissolved in 40 mL of deionized water to obtain a homogeneous solution. Similarly, 2-mIm (1.31 g, 16 mmol) was dissolved in 40 mL of deionized water to obtain a solution. Then, the aqueous solution of zinc salt was added into the aqueous solution of 2-mIm under vigorous stirring. After stirring for 3 h at RT, the product was collected by repeated centrifugation at 7000 rpm for 5 min and washed with fresh deionized water several times and finally dried at 80 °C under vacuum overnight.

3.3. Polymerization with ZIF-L

All polymerization reactions were executed under a dry and inert atmosphere using standard Schlenk techniques. A typical bulk polymerization was performed as follows. ZIF-L was first activated at 120 °C under the vacuum for 24 h, then a predetermined amount of activated ZIF-L and MMA were charged in a Schlenk flask under inert atmosphere. The flask was then purged with argon for a few minutes and sealed and immersed in the preheated oil bath and heated at a certain temperature. After polymerization at a constant temperature for a certain period of time, the reaction was terminated by cooling the flask in an ice bath and quenching in air as quickly as possible. Small aliquots were taken from the reaction mixture and quenched into around 0.6 mL CDCl_3 . The quenched aliquots were then analyzed by ^1H NMR, obtaining the monomer conversion. The resultant polymeric sample was then separated from the catalysts by dissolving in toluene and filtered. Afterwards, the pure polymeric sample was re-precipitated from methanol and washed repeatedly several times with fresh methanol, then dried at 60 °C under vacuum for 24 h and collected as a white solid.

3.4. Characterizations of Catalyst and Polymer

The powder X-ray diffraction (PXRD) spectrum was recorded with a Panalytical Empyrean instrument using monochromatic $\text{Cu K}\alpha$ radiation in the 2θ range of 3° to 60° at a scan rate of 2°/min. A scanning electron microscope (SEM) from JEOL (JSM-IT300, 0.5–35 kV) was used to determine the texture of ZIF-L. Thermogravimetric analysis (TGA) was carried out on a Netzsch (STA 449C) instrument (5 °C/min as heating rate) under N_2 atmosphere (20 mL/min) in the range of 25–800 °C for ZIF-L and 25–600 °C for polymeric substances. Differential scanning calorimetry (DSC) measurement was performed using NETZSCH STA 449C instrument under nitrogen flow. Fourier transform infrared spectroscopy (FT-IR) was performed using Bruker Vertex 80V ranging from 4000 to 400 cm^{-1} . The surface area and adsorption/desorption isotherms were measured using N_2 adsorption on Micromeritics ASAP 2020 equipment, and the sample (ZIF-L) was degassed at 200 °C for 3 h before measurement. The amount of acidic and basic sites of catalyst ZIF-8 were determined with temperature-programmed desorption (TPD) profile of NH_3 and CO_2 using Micromeritics chemisorb 2750 Pulse Chemisorption, respectively. ^1H -NMR spectra were recorded on a Bruker AC-500 using CDCl_3 as the solvent and tetramethylsilane (TMS) as the internal standard. The molecular weight (M_n) and molecular dispersity (\mathcal{D}) were measured by gel permeation chromatography (GPC) (PL-GPC 50 with PLgel 5 μm MIXED-C column, Agilent Technology) in THF using standard polystyrene as a standard. Matrix-assisted laser desorption ionization-time of flight mass spectroscopy (MALDI-TOF MS) of low molecular weight polymeric sample was performed using a Bruker ultrafleXtremeTM spectrometer. Moreover, an induced coupled plasma (ICP) test was performed for both the solution mixture and PMMA.

4. Conclusions

In summary, for the first time, the catalytic activity of a 2D MOF (ZIF-L) has been successfully investigated in the synthesis of ultrahigh molecular weight poly(methyl methacrylate) without any co-catalyst in solvent free-medium. Systematic analysis of the ZIF-L structure before and after the polymerization proves that it can polymerize methyl methacrylate at least three times without significant loss of its catalytic activity following the zwitterionic Lewis pair polymerization. In addition, the NMR, MALDI-TOF MS, and FTIR results demonstrated that PMMA is obtained with a six-membered lactone ring chain end, which formed through the intramolecular backbiting cyclization. Based on the ease of green synthesis and overall stability, this type of 2D MOF may be competitive not only with other MOFs but also with Lewis pairs for vinyl polymerization.

Supplementary Materials: The following supporting information can be downloaded at: <https://www.mdpi.com/article/10.3390/catal12050521/s1>, Figure S1: PXRD patterns of the synthesized and simulated ZIF-L (Zn); Figure S2: TGA curve of ZIF-L under N₂ flow (20 mL/min) ranging from 30 °C to 800 °C; Figure S3: The isotherms of nitrogen adsorption (filled symbols) and desorption (empty symbols) for the ZIF-L measured at -196 °C; Table S1: Bulk polymerization of MMA initiated with various Zn-salts, 2-mIm (ligand used for ZIF-L synthesis) and ZIF-L; Table S2: Amount of acid and basic sites of the catalyst (ZIF-L); Figure S4: Dependence of molecular weight (M_n), monomer conversion (%) and molecular dispersity (\bar{D}) on polymerization time (h) for MMA polymerization using ZIF-L(Zn); Figure S5: Dependence of molecular weight (M_n) and molecular dispersity (\bar{D}) on monomer conversion (%) for MMA polymerization using ZIF-L; Table S3: Chain-extension experiments of the polymerization of MMA at 140 °C; Figure S6: GPC traces of PMMA obtained from chain extension experiments; Figure S7: MMA conversion with polymerization time initiated by ZIF-L at 140 °C and [MMA]/[ZIF-L] = 50; Figure S8: ¹H-NMR spectra of (a) ZIF-L, (b) 2-mIm, (c) Zn(OAc)₂ and (d) ZnO mediated PMMA in CDCl₃ (Table 1) showing the intensity of CH₂ peaks of lactone at 1.64 ppm region; Figure S9: ¹H NMR spectra in both CDCl₃ of PMMA before (a) and after (b) adding acid anhydride; Figure S10: FT-IR spectra of monomer MMA and polymer PMMA obtained using ZIF-L as catalyst at 140 °C and [MMA]/[ZIF-L] = 50; Figure S11: DSC thermogram of PMMA (Table 1, entry 3) determined under N₂ flow; Figure S12: PXRD patterns of ZIF-L before and after the polymerization reaction. The compared results confirm the stability of the ZIF-L during polymerization; Figure S13: SEM micrographs of ZIF-L before (a) and after the polymerization reaction (b) (3rd cycle), Figure S14: The nitrogen adsorption–desorption isotherms of the recovered ZIF-L after the polymerization (3rd cycle) measured at 77K; Table S4: Elemental analysis (Zn metal) of the examined catalyst before and after the polymerization, mixture of solution, and synthesized PMMA using ICP method; Table S5: Recycling studies of the examined catalyst (ZIF-L).

Author Contributions: Conceptualization by M.A.R. and B.M., Methodology, analysis and writing—original draft preparation by M.A.R., Review and editing by B.M., F.N. and F.V. Supervision of the whole project by F.V. All authors have read and agreed to the published version of the manuscript.

Funding: This research was funded by the China Scholarship Council (CSC) (No. 2017GF001).

Acknowledgments: The authors are grateful to the State Key Lab of Advanced Technology for Materials Synthesis and Processing for financial support (Wuhan University of Technology). M.A.R. expresses his appreciations to the China Scholarship Council (CSC) for his PhD grant (No. 2017GF001) and to the Mawlana Bhashani Science and Technology University, Bangladesh, for the PhD study leave.

Conflicts of Interest: The authors declare no conflict of interest.

References

1. Yaghi, O.; Li, H. Hydrothermal synthesis of a metal-organic framework containing large rectangular channels. *J. Am. Chem. Soc.* **1995**, *117*, 10401–10402. [[CrossRef](#)]
2. Li, H.; Davis, C.E.; Groy, T.L.; Kelley, D.G.; Yaghi, O. Coordinatively unsaturated metal centers in the extended porous framework of Zn₃(BCD)₃·6CH₃OH (BCD = 1,4-benzenedicarboxylate). *J. Am. Chem. Soc.* **1998**, *120*, 2186–2187. [[CrossRef](#)]
3. Li, H.; Eddaoudi, M.; O’Keeffe, M.; Yaghi, O.M. Design and synthesis of an exceptionally stable and highly porous metal-organic framework. *Nature* **1999**, *402*, 276–279. [[CrossRef](#)]

4. Lin, R.-B.; Xiang, S.; Xing, H.; Zhou, W.; Chen, B. Exploration of porous metal–organic frameworks for gas separation and purification. *Coordin. Chem. Rev.* **2019**, *378*, 87–103. [[CrossRef](#)]
5. Chughtai, A.H.; Ahmad, N.; Younus, H.A.; Laypkov, A.; Verpoort, F. Metal–organic frameworks: Versatile heterogeneous catalysts for efficient catalytic organic transformations. *Chem. Soc. Rev.* **2015**, *44*, 6804–6849. [[CrossRef](#)]
6. Yang, D.; Gates, B.C. Catalysis by metal organic frameworks: Perspective and suggestions for future research. *ACS Catal.* **2019**, *9*, 1779–1798. [[CrossRef](#)]
7. Bavykina, A.; Kolobov, N.; Khan, I.S.; Bau, J.A.; Ramirez, A.; Gascon, J. Metal–organic frameworks in heterogeneous catalysis: Recent progress, new trends, and future perspectives. *Chem. Rev.* **2020**, *120*, 8468–8535. [[CrossRef](#)]
8. Koo, W.-T.; Jang, J.-S.; Kim, I.-D. Metal-organic frameworks for chemiresistive sensors. *Chem* **2019**, *5*, 1938–1963. [[CrossRef](#)]
9. Wang, D.; Jana, D.; Zhao, Y. Metal–organic framework derived nanozymes in biomedicine. *Accounts Chem. Res.* **2020**, sed from Aladdin Chemic53, 1389–1400. [[CrossRef](#)]
10. Chen, R.; Yao, J.; Gu, Q.; Smeets, S.; Baerlocher, C.; Gu, H.; Zhu, D.; Morris, W.; Yaghi, O.M.; Wang, H. A two-dimensional zeolitic imidazolate framework with a cushion-shaped cavity for CO₂ adsorption. *Chem. Commun.* **2013**, *49*, 9500–9502. [[CrossRef](#)]
11. Kang, Z.; Fan, L.; Sun, D. Recent advances and challenges of metal–organic framework membranes for gas separation. *J. Mater. Chem. A* **2017**, *5*, 10073–10091. [[CrossRef](#)]
12. Liu, W.; Yin, R.; Xu, X.; Zhang, L.; Shi, W.; Cao, X. Structural engineering of low-dimensional metal–organic frameworks: Synthesis, properties, and applications. *Adv. Sci.* **2019**, *6*, 1802373. [[CrossRef](#)] [[PubMed](#)]
13. Chakraborty, G.; Park, I.-H.; Medisetty, R.; Vittal, J.J. Two-dimensional metal-organic framework materials: Synthesis, structures, properties and applications. *Chem. Rev.* **2021**, *121*, 3751–3891. [[CrossRef](#)] [[PubMed](#)]
14. Chen, B.; Yang, Z.; Zhu, Y.; Xia, Y. Zeolitic imidazolate framework materials: Recent progress in synthesis and applications. *J. Mater. Chem. A* **2014**, *2*, 16811–16831. [[CrossRef](#)]
15. Gao, Y.; Qiao, Z.; Zhao, S.; Wang, Z.; Wang, J. In situ synthesis of polymer grafted zifs and application in mixed matrix membrane for CO₂ separation. *J. Mater. Chem. A* **2018**, *6*, 3151–3161. [[CrossRef](#)]
16. Zanon, A.; Verpoort, F. Metals@ZIFs: Catalytic applications and size selective catalysis. *Coordin. Chem. Rev.* **2017**, *353*, 201–222. [[CrossRef](#)]
17. Liu, J.; Goetjen, T.A.; Wang, Q.; Knapp, J.G.; Wasson, M.C.; Yang, Y.; Syed, Z.H.; Delferro, M.; Notestein, J.M.; Farha, O.K.; et al. Mof-enabled confinement and related effects for chemical catalyst presentation and utilization. *Chem. Soc. Rev.* **2022**, *51*, 1045–1097. [[CrossRef](#)]
18. Sun, C.-Y.; Qin, C.; Wang, X.-L.; Su, Z.-M. Metal-organic frameworks as potential drug delivery systems. *Expert Opin. Drug Del.* **2013**, *10*, 89–101. [[CrossRef](#)]
19. Liu, J.; Guo, Z.; Liang, K. Biocatalytic metal-organic framework-based artificial cells. *Adv. Funct. Mater.* **2019**, *29*, 1905321. [[CrossRef](#)]
20. Wang, T.; Kou, Z.; Mu, S.; Liu, J.; He, D.; Amiin, I.S.; Meng, W.; Zhou, K.; Luo, Z.; Chaemchuen, S. 2D dual-metal zeolitic-imidazolate-framework-(ZIF)-derived bifunctional air electrodes with ultrahigh electrochemical properties for rechargeable zinc–air batteries. *Adv. Funct. Mater.* **2018**, *28*, 1705048. [[CrossRef](#)]
21. Liu, Q.; Low, Z.-X.; Feng, Y.; Leong, S.; Zhong, Z.; Yao, J.; Hapgood, K.; Wang, H. Direct conversion of two-dimensional ZIF-L film to porous zno nano-sheet film and its performance as photoanode in dye-sensitized solar cell. *Micropor. Mesopor. Mat.* **2014**, *194*, 1–7. [[CrossRef](#)]
22. Zhong, Z.; Yao, J.; Chen, R.; Low, Z.; He, M.; Liu, J.Z.; Wang, H. Oriented two-dimensional zeolitic imidazolate framework-l membranes and their gas permeation properties. *J. Mater. Chem. A* **2015**, *3*, 15715–15722. [[CrossRef](#)]
23. Nasir, A.M.; Nordin, N.M.; Goh, P.; Ismail, A. Application of two-dimensional leaf-shaped zeolitic imidazolate framework (2D ZIF-L) as arsenite adsorbent: Kinetic, isotherm and mechanism. *J. Mol. Liq.* **2018**, *250*, 269–277. [[CrossRef](#)]
24. Gu, Q.; Ng, T.C.A.; Sun, Q.; Elshahawy, A.M.K.; Lyu, Z.; He, Z.; Zhang, L.; Ng, H.Y.; Zeng, K.; Wang, J. Heterogeneous ZIF-L membranes with improved hydrophilicity and anti-bacterial adhesion for potential application in water treatment. *RSC Adv.* **2019**, *9*, 1591–1601. [[CrossRef](#)]
25. Motevalli, B.; Taherifar, N.; Wang, H.; Liu, J.Z. Ab initio simulations to understand the leaf-shape crystal morphology of ZIF-L with two-dimensional layered network. *J. Phys. Chem. C* **2017**, *121*, 2221–2227. [[CrossRef](#)]
26. Low, Z.-X.; Yao, J.; Liu, Q.; He, M.; Wang, Z.; Suresh, A.K.; Bellare, J.; Wang, H. Crystal transformation in zeolitic-imidazolate framework. *Cryst. Growth Des.* **2014**, *14*, 6589–6598. [[CrossRef](#)]
27. Hong, M.; Chen, J.; Chen, E.Y.-X. Polymerization of polar monomers mediated by main-group lewis acid–base pairs. *Chem. Rev.* **2018**, *118*, 10551–10616. [[CrossRef](#)]
28. Nzahou Ottou, W.; Conde-Mendizabal, E.; Pascual, A.; Wirotius, A.-L.; Bourichon, D.; Vignolle, J.; Robert, F.; Landais, Y.; Sotiropoulos, J.-M.; Miqueu, K. Organic lewis pairs based on phosphine and electrophilic silane for the direct and controlled polymerization of methyl methacrylate: Experimental and theoretical investigations. *Macromolecules* **2017**, *50*, 762–774. [[CrossRef](#)]
29. Wang, X.; Zhang, Y.; Hong, M. Controlled and efficient polymerization of conjugated polar alkenes by lewis pairs based on sterically hindered aryloxide-substituted alkylaluminum. *Molecules* **2018**, *23*, 442. [[CrossRef](#)]
30. Zhang, Y.; Miyake, G.M.; Chen, E.Y.X. Alane-based classical and frustrated lewis pairs in polymer synthesis: Rapid polymerization of mma and naturally renewable methylene butyrolactones into high-molecular-weight polymers. *Angew. Chem. Int. Edit.* **2010**, *49*, 10158–10162. [[CrossRef](#)]

31. Zhang, Y.; Miyake, G.M.; John, M.G.; Falivene, L.; Caporaso, L.; Cavallo, L.; Chen, E.Y.-X. Lewis pair polymerization by classical and frustrated lewis pairs: Acid, base and monomer scope and polymerization mechanism. *Dalton T.* **2012**, *41*, 9119–9134. [[CrossRef](#)] [[PubMed](#)]
32. McGraw, M.L.; Chen, E.Y.-X. Lewis pair polymerization: Perspective on a ten-year journey. *Macromolecules* **2020**, *53*, 6102–6122. [[CrossRef](#)]
33. Wang, C.-G.; Chang, J.J.; Foo, E.Y.J.; Niino, H.; Chatani, S.; Hsu, S.Y.; Goto, A. Recyclable solid-supported catalysts for quaternary ammonium iodide-catalyzed living radical polymerization. *Macromolecules* **2020**, *53*, 51–58. [[CrossRef](#)]
34. Taskin, O.S.; Kiskan, B.; Yagci, Y. An efficient, heterogeneous, reusable atom transfer radical polymerization catalyst. *Polym. Int.* **2018**, *67*, 55–60. [[CrossRef](#)]
35. Yang, L.; Xie, C.; Li, Y.; Guo, L.; Nie, M.; Zhang, J.; Yan, Z.; Wang, J.; Wang, W. Polymerization of alkylsilanes on ZIF-8 to hierarchical siloxane microspheres and microflowers. *Catalysts* **2017**, *7*, 77. [[CrossRef](#)]
36. Luo, Z.; Chaemchuen, S.; Zhou, K.; Verpoort, F. Ring-opening polymerization of l-lactide to cyclic poly (lactide) by zeolitic imidazole framework ZIF-8 catalyst. *ChemSusChem* **2017**, *10*, 4135–4139. [[CrossRef](#)]
37. Mochizuki, S.; Kitao, T.; Uemura, T. Controlled polymerizations using metal–organic frameworks. *Chem. Commun.* **2018**, *54*, 11843–11856. [[CrossRef](#)]
38. Low, Z.-X.; Razmjou, A.; Wang, K.; Gray, S.; Duke, M.; Wang, H. Effect of addition of two-dimensional ZIF-L nanoflakes on the properties of polyethersulfone ultrafiltration membrane. *J. Membrane Sci.* **2014**, *460*, 9–17. [[CrossRef](#)]
39. Xue, S.; Jiang, H.; Zhong, Z.; Low, Z.-X.; Chen, R.; Xing, W. Palladium nanoparticles supported on a two-dimensional layered zeolitic imidazolate framework-l as an efficient size-selective catalyst. *Micropor. Mesopor. Mat.* **2016**, *221*, 220–227. [[CrossRef](#)]
40. Yang, C.; Zhang, W.; Wang, J.; Li, S.; Liu, X.; Dou, L.; Yue, T.; Sun, J.; Wang, J. Nanostructured morphology control and phase transition of zeolitic imidazolate frameworks as an ultra-high performance adsorbent for water purification. *Inorg. Chem. Front.* **2019**, *6*, 2667–2674. [[CrossRef](#)]
41. Lee, L.-H.; Chen, W.-C. High-refractive-index thin films prepared from trialkoxysilane-capped poly (methyl methacrylate)–titania materials. *Chem. Mater.* **2001**, *13*, 1137–1142. [[CrossRef](#)]
42. Samad, H.A.; Jaafar, M. Effect of polymethyl methacrylate (PMMA) powder to liquid monomer (P/L) ratio and powder molecular weight on the properties of pmma cement. *Polym-Plast. Technol.* **2009**, *48*, 554–560. [[CrossRef](#)]
43. Lu, Z.; Pan, Y.; Liu, X.; Zheng, G.; Schubert, D.W.; Liu, C. Molar mass and temperature dependence of rheological properties of polymethylmethacrylate melt. *Mater. Lett.* **2018**, *221*, 62–65. [[CrossRef](#)]
44. Xu, D.; Jin, J.; Chen, C.; Wen, Z. From nature to energy storage: A novel sustainable 3D cross-linked chitosan–PEGGE-based gel polymer electrolyte with excellent lithium-ion transport properties for lithium batteries. *ACS Appl. Mater. Inter.* **2018**, *10*, 38526–38537. [[CrossRef](#)]
45. Cheng, X.; Pan, J.; Zhao, Y.; Liao, M.; Peng, H. Gel polymer electrolytes for electrochemical energy storage. *Adv. Energy Mater.* **2018**, *8*, 1702184. [[CrossRef](#)]
46. Sun, J.; Li, Y.; Zhang, Q.; Hou, C.; Shi, Q.; Wang, H. A highly ionic conductive poly(methyl methacrylate) composite electrolyte with garnet-typed $\text{Li}_{6.75}\text{La}_3\text{Zr}_{1.75}\text{Nb}_{0.25}\text{O}_{12}$ nanowires. *Chem. Eng. J.* **2019**, *375*, 121922. [[CrossRef](#)]
47. D’Elia, A.; Deering, J.; Clifford, A.; Lee, B.; Grandfield, K.; Zhitomirsky, I. Electrophoretic deposition of polymethylmethacrylate and composites for biomedical applications. *Colloid. Surface B* **2020**, *188*, 110763. [[CrossRef](#)]
48. Meneghetti, P.; Qutubuddin, S.; Webber, A. Synthesis of polymer gel electrolyte with high molecular weight poly (methyl methacrylate)–clay nanocomposite. *Electrochim. Acta* **2004**, *49*, 4923–4931. [[CrossRef](#)]
49. Rzaev, J.; Penelle, J. Hp-raft: A free-radical polymerization technique for obtaining living polymers of ultrahigh molecular weights. *Angew. Chem. Inter. Edi.* **2004**, *43*, 1691–1694. [[CrossRef](#)]
50. Arita, T.; Kayama, Y.; Ohno, K.; Tsujii, Y.; Fukuda, T. High-pressure atom transfer radical polymerization of methyl methacrylate for well-defined ultrahigh molecular-weight polymers. *Polymer* **2008**, *49*, 2426–2429. [[CrossRef](#)]
51. Bai, Y.; He, J.; Zhang, Y. Ultra-high-molecular-weight polymers produced by the immortal phosphine-based catalyst system. *Angew. Chem.* **2018**, *130*, 17476–17480. [[CrossRef](#)]
52. Carmean, R.N.; Sims, M.B.; Figg, C.A.; Hurst, P.J.; Patterson, J.P.; Sumerlin, B.S. Ultrahigh molecular weight hydrophobic acrylic and styrenic polymers through organic-phase photoiniferter-mediated polymerization. *ACS Macro Lett.* **2020**, *9*, 613–618. [[CrossRef](#)]
53. Liu, G.; Jiang, Z.; Cao, K.; Nair, S.; Cheng, X.; Zhao, J.; Gomaa, H.; Wu, H.; Pan, F. Pervaporation performance comparison of hybrid membranes filled with two-dimensional zif-l nanosheets and zero-dimensional zif-8 nanoparticles. *J. Membrane Sci.* **2017**, *523*, 185–196. [[CrossRef](#)]
54. Zhu, W.; Li, X.; Sun, Y.; Guo, R.; Ding, S. Introducing hydrophilic ultra-thin zif-l into mixed matrix membranes for CO_2/CH_4 separation. *RSC Adv.* **2019**, *9*, 23390–23399. [[CrossRef](#)]
55. Zhang, S.; Du, M.; Shao, P.; Wang, L.; Ye, J.; Chen, J.; Chen, J. Carbonic anhydrase enzyme-MOFs composite with a superior catalytic performance to promote CO_2 absorption into tertiary amine solution. *Environ. Sci. Technol.* **2018**, *52*, 12708–12716. [[CrossRef](#)] [[PubMed](#)]
56. Zhang, F.; Dou, J.; Zhang, H. Mixed membranes comprising carboxymethyl cellulose (as capping agent and gas barrier matrix) and nanoporous zif-l nanosheets for gas separation applications. *Polymers* **2018**, *10*, 1340. [[CrossRef](#)]

57. Ding, B.; Wang, X.; Xu, Y.; Feng, S.; Ding, Y.; Pan, Y.; Xu, W.; Wang, H. Hydrothermal preparation of hierarchical zif-l nanostructures for enhanced co2 capture. *J. Colloid Interf. Sci.* **2018**, *519*, 38–43. [[CrossRef](#)]
58. Nadar, S.S.; Rathod, V.K. Encapsulation of lipase within metal-organic framework (MOF) with enhanced activity intensified under ultrasound. *Enzyme Microb. Technol.* **2018**, *108*, 11–20. [[CrossRef](#)]
59. Kim, J.; Kim, S.-N.; Jang, H.-G.; Seo, G.; Ahn, W.-S. CO₂ cycloaddition of styrene oxide over mof catalysts. *Appl. Catal. A Gen.* **2013**, *453*, 175–180. [[CrossRef](#)]
60. Naz, F.; Mumtaz, F.; Chaemchuen, S.; Verpoort, F. Bulk ring-opening polymerization of ϵ -caprolactone by zeolitic imidazolate framework. *Catal. Lett.* **2019**, *149*, 2132–2141. [[CrossRef](#)]
61. Garg, D.K.; Serra, C.A.; Hoarau, Y.; Parida, D.; Bouquey, M.; Muller, R. Analytical solution of free radical polymerization: Applications-implementing gel effect using ak model. *Macromolecules* **2014**, *47*, 7370–7377. [[CrossRef](#)]
62. He, J.; Zhang, Y.; Falivene, L.; Caporaso, L.; Cavallo, L.; Chen, E.Y.-X. Chain propagation and termination mechanisms for polymerization of conjugated polar alkenes by [al]-based frustrated lewis pairs. *Macromolecules* **2014**, *47*, 7765–7774. [[CrossRef](#)]
63. Jia, Y.-B.; Wang, Y.-B.; Ren, W.-M.; Xu, T.; Wang, J.; Lu, X.-B. Mechanistic aspects of initiation and deactivation in n-heterocyclic olefin mediated polymerization of acrylates with alane as activator. *Macromolecules* **2014**, *47*, 1966–1972. [[CrossRef](#)]
64. Peters, R.; Mengerink, Y.; Langereis, S.; Frederix, M.; Linssen, H.; van Hest, J.; van der Wal, S. Quantitation of functionality of poly(methyl methacrylate) by liquid chromatography under critical conditions followed by evaporative light-scattering detection: Comparison with nmr and titration. *J. Chromatogr. A* **2002**, *949*, 327–335. [[CrossRef](#)]
65. Chen, E.Y.-X. Polymerization by classical and frustrated lewis pairs. *Top. Curr. Chem.* **2013**, *334*, 239–260. [[PubMed](#)]
66. Pan, Y.; Liu, Y.; Zeng, G.; Zhao, L.; Lai, Z. Rapid synthesis of zeolitic imidazolate framework-8 (zif-8) nanocrystals in an aqueous system. *Chem. Commun.* **2011**, *47*, 2071–2073. [[CrossRef](#)]
67. Yao, J.; He, M.; Wang, H. Strategies for controlling crystal structure and reducing usage of organic ligand and solvents in the synthesis of zeolitic imidazolate frameworks. *CrystEngComm* **2015**, *17*, 4970–4976. [[CrossRef](#)]